Nanoscale

Accepted Manuscript

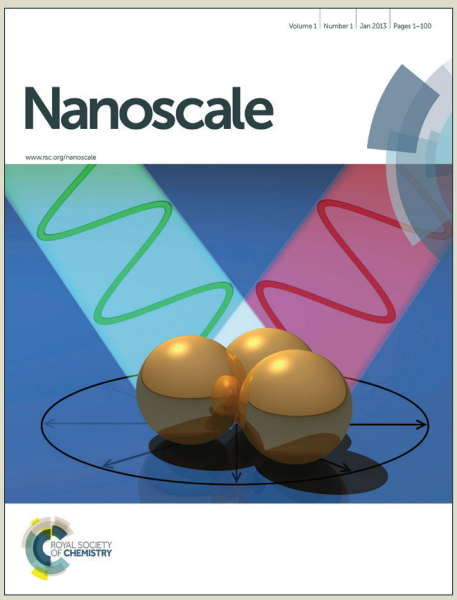

ROYAL SOCIETY OF CHEMISTRY

www.rsc.org/nanoscale

Journal Name

ARTICLE

ILs-derived N, S Co-doped Ordered Mesoporous Carbon for High-Performance Oxygen Reduction

Received 00th January 20xx,
Accepted 00th January 20xx

Wenxiu Yang, Xiaoyu Yue, Xiangjian Liu, Junfeng Zhai, and Jianbo Jia *

DOI: 10.1039/x0xx00000x

www.rsc.org/

A high efficient N, S co-doped porous carbon ORR catalyst was simply designed in our report from ordered mesoporou carbon (OMC) and trace ion liqiuds (ILs). The microstructure OMC was choosed as the template for improving the specif area, confining the ILs in the mesopores, and promoting the formation of the planar N and S doping. The resulting ILs/OM (IOMC) nanostructure exhibits comparable ORR activity and better stability than the commercial Pt/C catalyst in 0.10 M KOH solution, which make it one of the best-performing metal-free carbon ORR catalysts. We deduce that the exce ORR activity is attributed to the synergistic effect of N, S, and the order mesoporous structure. Interestingly, the O activity can be further boosted in both basic and acidic solutions after Fe doping into the IOMC nanostructures which clearly emphasizes transition metal Fe is important for the construction of ORR active functional sites especially in acidi solution.

Introduction

It is a top priority to rationally design and produce the advanced oxygen reduction reaction (ORR) catalysts to promote the development and application of fuel cells. Ordinarily, a superior and cheap ORR catalyst always possesses the following characteristics: (1) High specific surface area, which is a potential solution to improve surface density of catalytic sites.[1-3] (2) Controlled microstructures. Classically, carbon dot, 1D nanowire, 2D graphene-like plane, and 3D carbon composite framework, possess different ORR activity due to their unique microstructures. [4, 5] (3) High efficient catalytic sites. Heteroatom and transition metal doping have been regarded as an excellent method to promote the efficient of catalytic sites. [6, 7] (4) Good conductivity and stability.

Heteroatom doped carbon materials, due to their unique physical and chemical characteristics, have been studied for many years as the ORR catalysts since Jasinski's report on the ability of metal-N_4 macrocycle as ORR catalyst precursors.[8] Among the doped carbon materials, electronegative N atom is by far the "star doping atom" which induces structural deformation, increases asymmetries of charge, spin densities, and electron transfer ability.[9-11] Interestingly, there is a synergistic effect between the different heteroatoms co-doped carbon materials that can improve the catalytic activity for ORR.[12] Among all other co-doping elements with N, S is particularly attractive due to its larger atomic radius than that of N c C which might induce more strains and defects.[13] Meanwhile, tw lone pair electrons of S may contribute to interaction with O_2 during the ORR process.[14] Moreover, it has been demonstrated that S-dope graphene can exhibit better metallic properties than the pristine graphene sheet.[15]

Traditional synthesis methods involve NH_3 etching the carbo material or the carbonization of the heteroatom-containing precursors such as polymer, small molecule, and biomass resource *etc.*, all of which exist the bottleneck including uncontrolle microstructures, low yield, and complex synthesis procedure.[16-19] Ionic liquids (ILs) are a type of molten salts usually possessi negligible vapor pressure and versatile solvation properties which are benefit for the pyrolysis process.[20, 21] Dai's group has reported that microporous and mesoporous carbons can be prepared from tas specific ILs which can undergo cross-linking reactions under pyrolysis conditions.[22] Furthermore, they also found that functional porous carbon and carbon–oxide composite materials can be g from conventional ILs by confined carbonization.[23] Moreover, Sun's group discovers one-pot synthesis of a new family of mesoporou Fe-N-C catalyst from Fe-IL/N-IL precursors.[10] However, too much ILs was consumed in their studies. Meanwhile, complicated proce was used in their reports due to the hard template must be removed after the pyrolysis. Last but not least, the ORR activity of the meta free carbon composites still inferior to the commercial Pt/C.

Herein, we report a simple method to design a high efficient N, S c doped porous carbon ORR catalyst from ordered mesoporous carbo (OMC) and trace ILs. We choose the OMC as the template f improving the specific area of the resulting material, while the act as heteroatom containing molecules for the co-doping of N and

State Key Laboratory of Electroanalytical Chemistry, Changchun Institute of Applied Chemistry, Chinese Academy of Sciences, Changchun 130022, China
University of Chinese Academy of Sciences, Beijing 100049, China
Corresponding Authors: jbjia@ciac.ac.cn (J. Jia)
Electronic supplementary information (ESI) available: Supplementary figures and tables. See DOI:

Journal Name

ARTICLE

In our design, the microstructure of the OMC also confines the ILs in the mesopores, promotes the formation of the planar N and benefits for S doping. The resulting ILs/OMC (IOMC) nanostructures show excellent ORR electrocatalytic activity, which was confirmed by their positive half-wave potential, high limited current density, and durability in alkaline media. Interestingly, the ORR activity can be further boosted in both basic and acidic solutions after Fe doping into the IOMC nanostructures.

Experimental Section

Materials: Ordered mesoporous carbon CMK-3 was purchased from the Nanjing XFNANO Materials Tech Co., Ltd (XFNANO). Pt catalyst (20 wt %, Pt/C) was purchased from Johnson Matthey. Methanol and iron nitrate were obtained from Beijing Chemical Reagent Company (Beijing, China). 1-Butyl-1-methylpyrrolidinium bis(trifluoromethylsulfonyl)imide ([BMP][TFSA]) was purchased from Aladdin. 1-Butyl-1-methylpyrrolidinium dicyanamide (BMPyrDCA) was got from Sigma–Aldrich. All aqueous solutions were prepared with ultrapure water from a Water Purifier System (Sichuan Water Purifier Co. Ltd., China).

Apparatus: X-Ray diffraction (XRD) data were obtained with model D8 ADVANCE (BRUKER, Cu Kα radiation, λ =1.5406 Å). Transmission electron microscopy (TEM) was measured with a JEM-2100F high-resolution transmission electron microscope (JEOL Ltd., Japan). X-Ray photoelectron spectroscopy (XPS) analysis was performed on an ESCALABMKII X-ray photoelectron spectrometer (VG Scientific, UK). Nitrogen sorption isotherms were obtained with an ASAP 2020 Physisorption Analyzer (Micrometrics Instrument Corporation). Raman spectra were measured with a Renishaw 2000 model confocal microscopy Raman spectrometer with a CCD detector and a holographic notch filter (Renishaw Ltd., Gloucestershire, U. K.). The electrochemical impedance spectroscopy (EIS) measurements were got by a Zennium electrochemical workstation (Zahner, Germany). The electrochemical experiments were employed using a CHI842B electrochemical workstation (CH Instruments, Shanghai). Rotating ring-disk electrode (RRDE) techniques were performed on a Model RRDE-3A Apparatus (ALS, Japan) with CHI842B electrochemical workstation. The electrochemical experiments were carried out via a three electrode system with a modified glassy carbon electrode (GCE, φ = 3.0 mm) as the working electrode, an Ag/AgCl (saturated KCl) electrode as the reference electrode, and a platinum foil as the counter electrode, respectively. All the electrochemical measurements were carried out at room temperature.

Synthesis of IOMC-X composites:

In a typical synthesis of IOMC-850, 70 μl of [BMP][TFSA] was dropped into 0.0300 g of OMC, and then grinding them in an agate mortar for several minutes. The remaining mixture was heated at 180, 240, and 850 °C for 2, 2, and 2 h at a heating rate of 2 °C/min respectively in a quartz boat in nitrogen. To clarify, the resulting sample was labeled as IOMC-850 considering the use of ILs, OMC and the pyrolysis temperature (850 °C).

For further Fe doping, the resulting IOMC-850 was impregnated with 1.0 wt.% $Fe(NO_3)_3$ aqueous, and dried at 50 °C. The mixture was heated in N_2 at a rate of 2 °C/min to 180, 240, and 800 °C and held at that temperature for 2, 2, and 1 h, respectively. The resulting sample was named as Fe-IOMC.

To further testify the synergistic effect of the co-doping N and S, we prepared the N-IOMC-850 which just contains N atom from BMPyrDCA (without S) and OMC under the same conditions.

Electrocatalytic activity evaluation:

Before modification, the GCE was polished carefully with 0.3 μm alumina slurries, followed by sonication in acetone, ethanol and ultrapure water successively, and then allowed to dry at room temperature. For a typical procedure, 4.0 mg of the IOMC-850 sample or Pt catalyst (20 wt %, Pt/C) were dissolved in a mixture (4 ml) of water, isopropyl alcohol, and Nafion (5.0 wt %) with a ratio of 20:1:0.075 (v/v/v) under sonication, respectively. For electrochemical measurements, a certain amount of the IOMC-850 suspension was dropped onto the pretreated electrode surface (500 μg/cm^2), and the modified electrode was denoted as the IOMC-850/GCE. The modified electrodes were dried under the infrared lamp before use. For comparison, the Pt/C/GCE was prepared according to the same procedure with suitable amount of catalyst (25 μg Pt/cm^2).

For RRDE experiments, the O_2 reduction voltammogram was obtained by performing a negative-direction sweep of potential from 0.2 V in 0.10 M KOH or from 0.8 V in 0.10 M $HClO_4$ at a rate of 5 mV/s, and the ring potential was set at 0.3 V in 0.10 M KOH or 1.0 V in 0.10 M $HClO_4$, respectively. Before experiments, all the electrodes were activated by potential cycling in 0.10 M $HClO_4$ from 1.0 to −0.4 V at a scan rate of 50 mV/s for 30 cycles.

Results and discussion

The hybrid's microstructure was first characterized by transmission electron microscopy (TEM) to compare the morphological changes of the IOMC synthesized at different temperatures. As displayed in **Fig. 1a and S1**, the microstructures of IOMCs are similar to the commercial pure OMC. The results indicated that the doping and

Journal Name

ARTICLE

pyrolysis at different temperatures only led to different thin carbon films on the surface of the mesoporous structure. As shown in **Fig. 1b and c**, we further investigate the elemental distribution of a typical IOMC-850 by high-angle annular dark-field scanning transmission electron microscopy (HAADF-STEM). It is obvious that C (red), N (orange), S (green), and O (yellow) uniformly distribute on the whole surface of the IOMC-850. **Fig. 1d** exhibits XRD of the resultant IOMC-850, which is agreed to that of OMC. Briefly, a typical peak at about 26° is observed, corresponding to the (002) facets of graphite carbon. Therefore, combining the results of TEM with XRD, mesopore structure does remain after the pyrolysis procedure. Raman spectrum was carried out to study the degree of graphitization of the IOMC-850 samples because the D band (1360 cm^{-1}) and G band (1590 cm^{-1}) provide information about the disorder and crystallinity of sp^2 carbon, respectively. Meanwhile, the ratio of D band to G band (I_D/I_G) of a carbon material can be used to estimate the degree of graphitization. As given in **Fig. 1e and Table S1**, IOMC-850 shows the highest I_D/I_G value of 1.05 compare with OMC (0.94) and N-IOMC-850 (0.98), indicating a high degree of disordered carbon, which can be attributed to the co-doping of N and S.

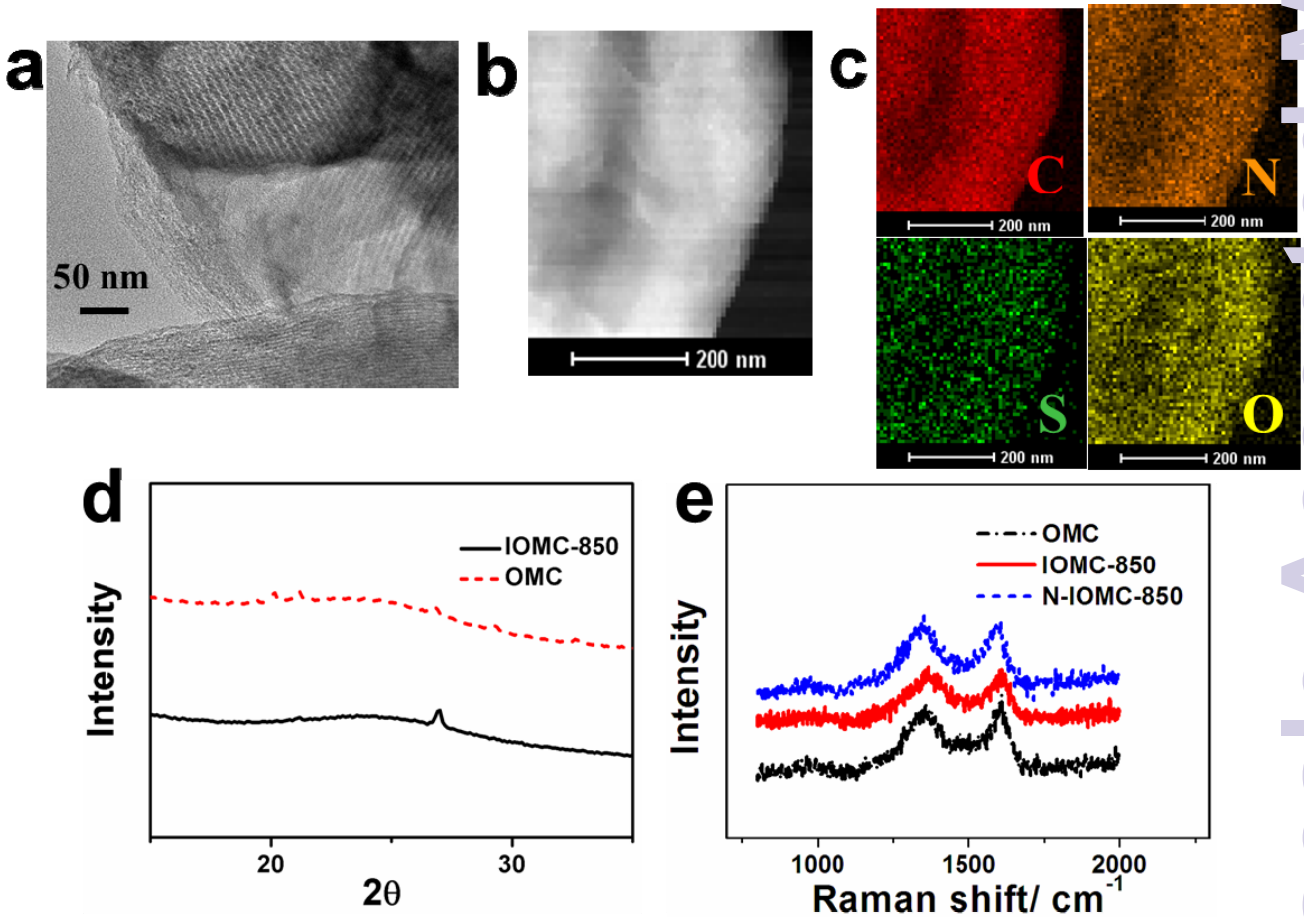

Fig. 1 a) TEM image, (b) HAADF-STEM, and (c) its mapping images of the resultant IOMC-850, d) XRD, and e) Raman images of the resultant materials.

The porosity of the materials was explored by means of nitrogen sorption technique (**Fig. 2a and S2**). The nitrogen adsorption-desorption isotherms of IOMC-850 show the biggest BET surface area (666.1 m^2 g^{-1}) in all the investigated IOMC samples which is comparable to that of OMC (749.1 m^2 g^{-1}) (**Table S2**). **Fig. 2b** displays that the mesopore diameter of IOMC-850 calculated by Barrett-Joyner-Halenda (BJH) desorption method is ca. 3.88 nm while diameter of the OMC is 4.18 nm. The decrease of the mesopore diameter may be due to the doping of ILs which was incorporated in the mesopores of OMC (**Fig. S2**). XPS analysis (**T**

2c) reveals that IOMC-850 is mainly composed of C (88.99 at.%), N (0.91 at.%), O (9.43 at.%), and S (0.67 at.%), confirming that N and S have been successfully doped into the IOMC composite. As shown in **Fig. 2d**, the high-resolution XPS of S2p can be resolved into three different peaks at 163.9, 165.1, and 168.3 eV which should be attributed to 2p 3/2 and 2p 1/2 peaks of thiophene–S (87.9 at.%), and $–SO_x–$ (x= 2–4, 12.1 at.%), respectively.[13] Hence, S is inferred to be mainly doped at the edges or on the surface of OMC in the form of −C−S−C− or $−C−SO_X−C−$.[24] Meanwhile, because S has a larger atomic radius (103 pm) than C (77 pm), more strains and defects can be introduced into the carbon matrix which will increase the conductivity of porous carbon and facilitate charge localization for favorable O_2 chemisorption.[13-15, 25] Moreover, a high-resolution N 1s XPS spectrum of IOMC-850 (**Fig. 2e**) depicts that there exists pyridinic, pyrrolic, and graphitic N. The amount of planar N (pyridinic and pyrrolic N) has been determined to be *ca.* 60%. Therefore, we deduce that the high proportion of doped planar N in IOMC-850 probably leads to the increase of current density, spin density, and the density of π states of carbon atoms near the Fermi level, thus enhancing intrinsic ORR activity.[26, 27] At l… electrochemical impedance spectroscopy (EIS) analysis wa… conducted in the frequency from 100 mHz to 100 kHz in 5.0 mM $[Fe(CN)_6]^{3-/4-}$ containing 0.10 M KCl to verify electronic conductivity of the IOMC-850, N-IOMC-850 and OMC. **Fig. 2f** exhibits the Nyquist plots of the IOMC-850/GCE, N-IOMC-850/GCE, OMC/GCE, and bare GCE, respectively. The absence of the semicircle regions in the plots confirms the low faradic resistances of the modified GCE.[17] Meanwhile, the intern… resistances increased in the order of IOMC-850/GCE< N-IOMC-850/GCE < OMC/GCE < bare GCE. Therefore, combine of Rama… and EIS, the doping of heteroatoms (N and S) could efficientl… enhance the defects density and conductivities of the resultin… composites, which benefit for the improvement of ORR catalyt… activity compare with pure OMC.

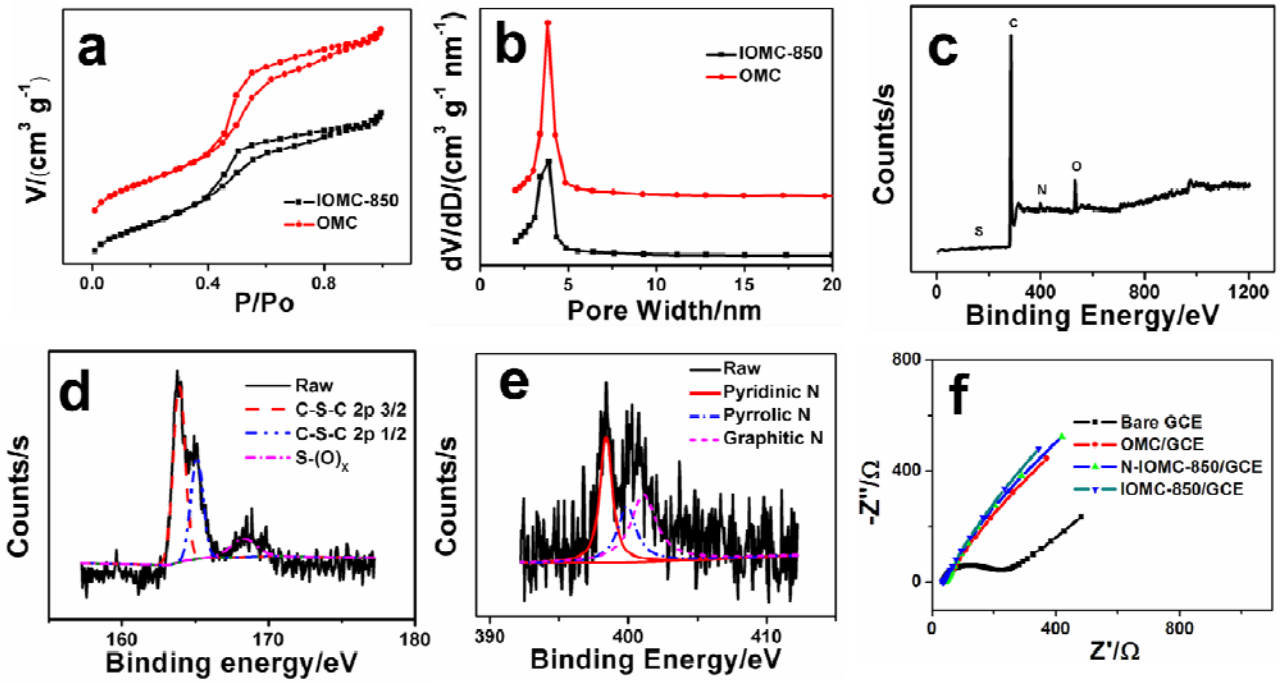

Fig. 2 a) N_2 adsorption/desorption isotherm, (b), the pore size distribution of the IOMC-850 and OMC. (c) XPS survey, high-resolution (d) … 2p and (e) N1s XPS spectrum for the resultant IOMC-850. (f) EIS of the different materials.

The electrocatalytic activities for ORR of the as-synthesized IOMC materials were studied by rotating disk electrode (RDE) and rotating ring-disk electrode (RRDE) techniques. As presented in **Fig. 3a**, relative to IOMC-700, IOMC-800, and IOMC-900, IOMC-850 performs best ORR activity with more positive onset potential (E_{onset}) and half-wave potential ($E_{1/2}$) in O_2-saturated 0.10 M KOH. **Fig. 3b** shows typical RRDE voltammograms of IOMC-850 and commercial 20% Pt/C catalyst obtained in O_2-saturated 0.10 M KOH solution at room temperature. Interestingly, metal-free carbon composite (IOMC-850) shows comparable ORR electrocatalytic activity to commercial Pt/C which makes it as one of best metal-free ORR catalysts ever reported in alkaline solution. Briefly, the IOMC-850 exhibits a high $E_{1/2}$ (ca. -0.155 V), which is close to that of the Pt/C catalyst (-0.152 V), meanwhile, the E_{onset} of the IOMC-850 (0.009 V) is same as that of Pt/C catalyst. The H_2O_2 yield on the IOMC-85… catalyst in basic solution is below 9.8% over the whole potential range investigated (**Fig. 3c**), corresponding to a high electron transfer number of ca. 3.9 (**Fig. 3d**), which is close to that of Pt/C catalyst. These results indicate the IOMC-850 possesses excelle… t electrocatalytic activity and achieves $4e^-$ pathway dominated ORR process. Furthermore, IOMC-850 also performs high stability f… ORR in alkaline solution, as confirmed by none of the linear sweep voltammetric (LSV) curve shift after 3000 cycles between 0.2 to -0… V (**Fig. 3e**), while the $E_{1/2}$ of the Pt/C catalyst negatively shifts 2… mV under the same conditions (**Fig. 3f**), which suggest superi… durability of the IOMC-850 catalyst.

Based on the above morphological, compositional, and electrochemical characterizations of IOMC-850, we conclude that four important aspects should be responsible for its superior ORR activity and stability: (1) The OMC substrate not only increases the specific surface area and electronic conductivity of the resulting carbon composites, but also offers more active sites for co-doping of heteroatoms and ORR. (2) High percentage of planar N (60%) doped into the IOMC-850 can promote O_2 adsorption due to the reduced the local work function of carbon.[28, 29] (3) The doping of S atom in IOMC-850. So far, many reports have focused on the

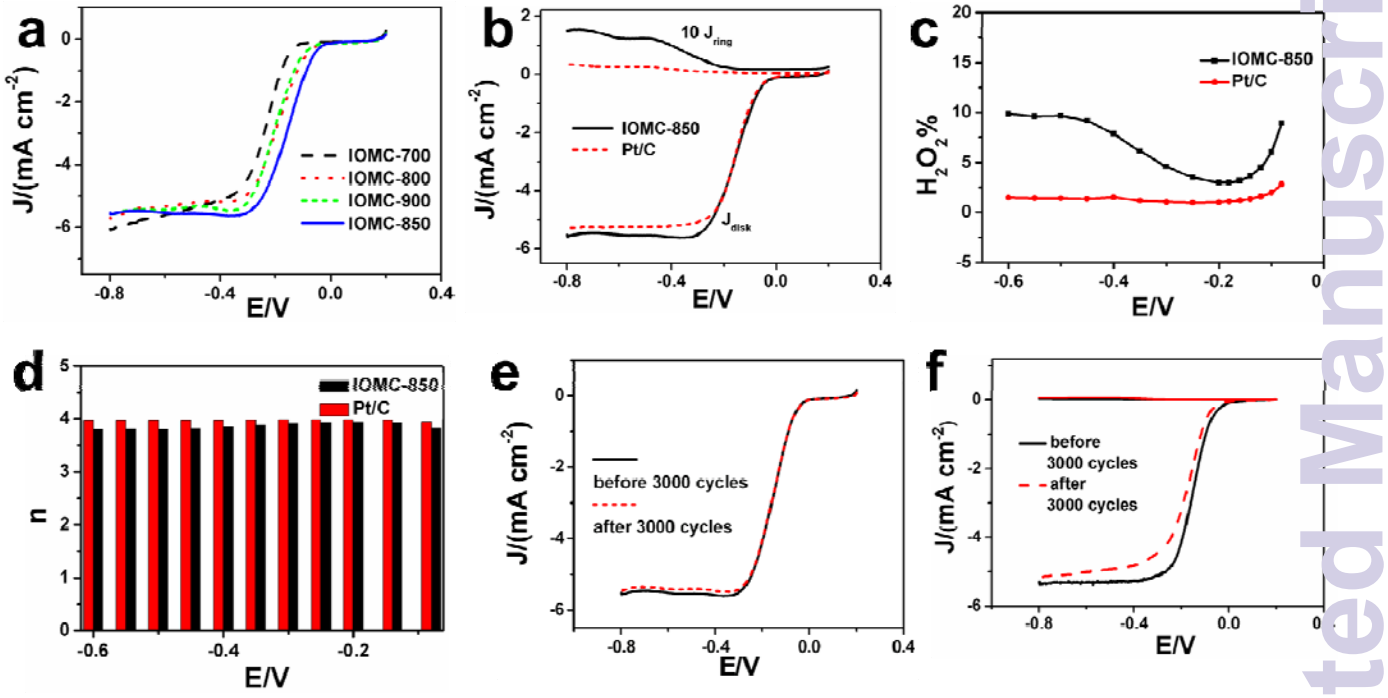

Fig. 3 a) LSV curves of different materials, b) RRDE voltammograms, c) H_2O_2 % yield, and d) electron transfer number (n) of IOMC-850 and Pt/C in O_2-saturated 0.10 M KOH at a scan rate of 5 mV/s, rotation rate of 1600 rpm. LSV curves of (e) IOMC-850 and (f) Pt/C for ORR in O_2-saturated 0.10 M KOH before and after 3000 cycles.

positive effect of S atom toward the ORR.[12, 30] Briefly, it has been demonstrated that S-doping has aroused formation of more disorders in the carbon framework and enhanced electronic conductivity. [15, 24] (4) The synergistic effect of the co-doping N and S. It has been reported that the origin inert carbon π electrons can be activated through conjugation with lone-pair electrons of electronegativity atoms such as N, S, F, *etc*.[28] Moreover, Paraknowitsch's group has demonstrated that the role of N in changing the electronic structure of pure carbon not only can be transferred to other heteroatoms, but also can be improved, such as in the N−S sample.[12] In addition, the introduction of S to N-doped carbon increases the portion of pyridinic-N sites, creates asymmetrical spin and charge density and causes the synergetic effect of N and S, which facilitates the ORR.

In a word, the excellent electrocatalytic activity and long-term stability of IOMC-850 owe to the synergistic effect of N, S, and the ordered mesoporous structure. This makes it one of the best metal-free heteroatom doped carbon catalyst ever reported for ORR in alkaline solutions (**Table S3**). To further verify the synergistic effect of the co-doped N and S, the N-IOMC-850 which is free of S was checked. As displayed in **Fig. S3**, the N-OMC-850 catalyst shows inferior ORR activity which $E_{1/2}$ negatively shifts 57 mV compare with N, S co-doped IOMC-850.

For further improving the ORR activity of the IOMC system, we prepared the Fe-IOMC by adding Fe into the IOMC-850. As displayed in **Fig. S4**, there are many mono-dispersed black dots (diameter ca. 10 nm) on the surface of the Fe-IOMC and only few of them aggregated, demonstrating Fe-based nanoparticles were formed during the thermal treatment at 800 °C. Interestingly, the ORR catalytic activity of Fe-IOMC increased significantly in both basic and acidic solutions compared with those of IOMC-850. **Fig. 4a** shows that the E_{onset} and $E_{1/2}$ of Fe-IOMC positively shifted *ca.* 1 and 20 mV in 0.10 M KOH relative to those of the IOMC-850 respectively. Moreover, **Fig. 4b** shows typical RRDE voltammograms of Fe-IOMC and commercial Pt/C catalyst obtained at room temperature in O_2-saturated 0.10 M $HClO_4$ solution. We found that Fe-IOMC shows comparable electrocatalytic activity toward ORR to the commercial Pt/C, which E_{onset} and $E_{1/2}$ are *ca.* 0.571 and 0.313 V, respectively. Overall, in addition to the heteroatoms of N and S, Fe also plays a key role in the ORR catalysts especially in acidic solution.

Journal Name

ARTICLE

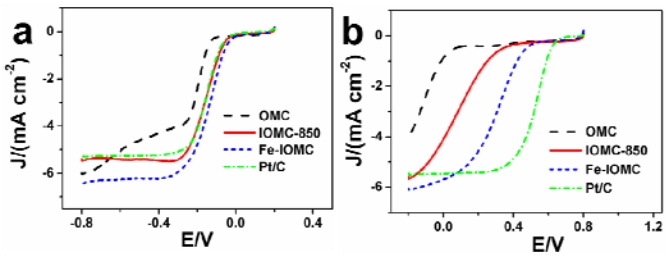

Fig. 4 LSV curves of different materials in O_2-saturated (a) 0.10 M KOH and (b) 0.10 M $HClO_4$ at a scan rate of 5 mV/s, rotation rate = 1600 rpm.

In summary, we developed a new simple and economical synthetic strategy for the controlled synthesis of heteroatom-doping metal–free mesoporous carbon hybrids by pyrolysis of the mixture of OMC and ILs ([BMP][TFSA]). We found that OMC not only amplifies the specific surface area and electronic conductivity of the resulting IOMC materials, but also offers more sites for the co-doping of N and S which will reduce the consumption of ILs. The IOMC-850 exhibits comparable ORR activity and better stability than the commercial Pt/C catalyst in 0.10 M KOH solution, which make it one of the best-performing metal-free carbon ORR catalysts. We deduce that the excellent ORR activity is attributed to the synergistic effect of N, S, and the order mesoporous structure. Additionally, we found doping Fe into IOMC-850 could further improve the ORR activity which clearly emphasizes transition metal Fe is important for the construction of ORR active functional sites especially in acidic solution. Accordingly, this rational design and integration provide a new avenue to construct novel carbon hybrid with tunable catalytic properties and open new ideas for the application of stable heteroatoms-doping composite materials in fuel cells, lithium-ion batteries, sensors, and supercapacitors.

Acknowledgement

We acknowledge financial supports from the Ministry of Science and Technology of China (No. 2013YQ170585).

References

1. S. Guo, S. Zhang and S. Sun, *Angew. Chem., Int. Ed.*, 2013, **52**, 8526.
2. H. Shi, Y. Shen, F. He, Y. Li, A. Liu, S. Liu and Y. Zhang, *J. Mater. Chem. A*, 2014, **2**, 15704.
3. F. Jaouen, E. Proietti, M. Lefèvre, R. Chenitz, J.-P. Dodelet, G. Wu, H. T. Chung, C. M. Johnston and P. Zelenay, *Energ. Environ. Sci.*, 2011, **4**, 114.
4. H. X. Zhong, J. Wang, Y. W. Zhang, W. L. Xu, W. Xing, D. Xu, Y. F. Zhang and X. B. Zhang, *Angew. Chem., Int. Ed.*, 2014, **53**, 14235.
5. T. Y. Ma, S. Dai, M. Jaroniec and S. Z.Qiao, *J. Am. Chem. Soc.*, 2014**, 136**, 13925.
6. Y. Hu, J. O. Jensen, W. Zhang, L. N. Cleemann, W. Xing, N. J. Bjerrum and Q. Li, *Angew. Chem., Int. Ed.*, 2014, **53**, 3675.
7. J. Liang, Y. Jiao, M. Jaroniec and S. Z. Qiao, *Angew. Chem., Int. Ed.*, 2012, **51**, 11496.
8. R. Jasinski, *Nature*, 1964, **201**, 1212.
9. A. G. Kannan, J. Zhao, S. G. Jo, Y. S. Kang and D.-W. Kim, *J. Mater. Chem. A*, 2014, **2**, 12232.
10. Z. Li, G. Li, L. Jiang, J. Li, G. Sun, C. Xia and F. Li, *Angew. Chem., Int. Ed.*, 2015, **54**, 1494.
11. W. Yang, T. P. Fellinger and M. Antonietti, *J. Am. Chem. Soc.*, 2011, **133**, 206.
12. N. Ranjbar Sahraie, J. P. Paraknowitsch, C. Gobel, A. Thomas and P. Strasser, *J. Am. Chem. Soc.*, 2014, **136**, 14486.
13. R. Zheng, Z. Mo, S. Liao, H. Song, Z. Fu and P. Huang, *Carbon*, 2014, **69**, 132.
14. W. Kiciński, M. Szala and M. Bystrzejewski, *Carbon*, 2014, **68**, 1.
15. G. Ning, X. Ma, X. Zhu, Y. Cao, Y. Sun, C. Qi, Z. Fan, Y. Li, Y. Zhang, X. Lan and J. Gao, *ACS Appl. Mater. Inter.*, 2014, **6**, 15950.
16. D. Liu, X. Zhang, Z. Sun and T. You, *Nanoscale*, 2013, **5**, 9528.
17. W. Yang, Y. Zhang, C. Liu and J. Jia, *J.Power Sources*, 2015, **274**, 595.
18. J. Liang, R. F. Zhou, X. M. Chen, Y. H. Tang and S. Z. Qiao, *Adv. Mater.*, 2014, **26**, 6074.
19. W. Yang, Y. Zhai, X. Yue, Y. Wang and J. Jia, *Chem. Commun.*, 2014, **50**, 11151.
20. S. Zhang, M. S. Miran, A. Ikoma, K. Dokko and M. Watanabe, *J. Am. Chem. Soc.*, 2014, **136**, 1690.
21. Y. She, Z. Lu, M. Ni, L. Li and M. K. Leung, *ACS Appl. Mater. Inter.*, 2015, **7,** 7214.
22. J. S. Lee, X. Wang, H. Luo, G. A. Baker and S. Dai, *J. Am. Chem. Soc.*, 2009, **131**, 4596.
23. X. Wang and S. Dai, *Angew. Chem., Int. Ed.*,2014, **53**, 4102.
24. L. Zhang, J. Niu, M. Li and Z. Xia, *J. Phys.Chem. C*, 2014, **118**, 3545.
25. U. N. Maiti, W. J. Lee, J. M. Lee, Y. Oh, J. Y. Kim, J. E. Kim, J. Shim, T. H. Han and S. O. Kim, *Adv. Mater.*, 2014, **26,** 40.
26. W. Yang, X. Liu, X. Yue, J. Jia and S. Guo, *J.Am. Chem. Soc.*, 2015, **137**, 1436.
27. K. Gong, F. Du, Z. Xia, M. Durstock and L. Dai, *Science*, 2009, **323**, 760.
28. W. Ding, Z. Wei, S. Chen, X. Qi, T. Yang, J. Hu, D. Wang, L.-J. Wan, S. F. Alvi and L. Li, *Angew. Chem., Int. Ed.*, 2013, **52**, 11755.
29. Z. Luo, S. Lim, Z. Tian, J. Shang, L. Lai, B. MacDonald, C. Fu, Z. Shen, T. Yu and J. Lin, *J. Mater. Chem.*, 2011, **21**, 8038.
30. K. Mamtani and U. S. Ozkan, *Catal. Lett.*, 2015, **145**, 436.